TITLE: CD2 expression is co-regulated with stemness- and exhaustion-associated factors in human T cells

Authors: Philippos Demetriou[1*], Maria Iakovou[1], Gregoria Gregoriou[1], Dimitris Vrachnos[2], Jianxiang Chi[1], Vasilia Tamamouna[1,3,4], Stavros Constantinou[5], Vakis Papanastasiou[5], Athos Antoniades[2], Paul Costeas[1,6]

Affiliations:

[1]The Center for the Study of Haematological and Other Malignancies, Nicosia, Cyprus.

[2] Stremble Ventures LTD, Limassol, Cyprus.

[3] Cambridge Stem Cell Institute, University of Cambridge, Cambridge, United Kingdom.

[4] Department of Haematology, University of Cambridge.

[5] Aretaeio Hospital, 55-57 Andrea Avraamides, Strovolos, 2024 Nicosia, Cyprus.

[6] Cyprus Cancer Research Institute, Aglantzia, Nicosia, Cyprus.

*Corresponding author. Email: demephil@gmail.com, The Center for the Study of Haematological Malignancies, Nicosia, Cyprus.

ABSTRACT

The CD2-CD58 pathway has been highlighted as a major player in anti-tumour T cell immunity. Our study reveals that CD2 costimulation strength significantly correlates with T cell activation, the average number of cell divisions, fold expansion, and IFN-γ production. Our findings suggest that the correlation of CD2 strength with the level of CD25 expression is a potential regulatory mechanism by which CD2 strength enhances above proliferation parameters. We find that human brain cancer tumour-infiltrating CD8+ and CD4+ T cells exhibit reduced levels of CD2, suggestive of a compromised CD2 strength upon CD2 engagement. Through a genome-wide CRISPR-Cas9 knockout screen, we identified two epigenetic regulators, SUZ12 and BAP1, as positive modulators of CD2 expression. We demonstrate that BAP1 is crucial for the upregulation and sustained high expression of CD2 following T cell activation. We reveal that CD2 is co-regulated with other co-stimulatory/inhibitory receptors, and factors associated with T cell stemness and exhaustion, in a dose-dependent manner. Importantly, we rescue the loss of CD2 due to BAP1 knockout by pharmacological inhibition of histone deacetylases making this a harnessable regulatory pathway. The insight from our study enhance our understanding of CD2-mediated T cell regulation and identify essential regulators of this pathway.

58 **INTRODUCTION**

59 The interplay between costimulatory and coinhibitory receptors on T cells is crucial for
60 determining downstream T cell activation and responses[1,2]. Immunotherapy strategies aimed
61 at enhancing T cell immunity against cancer have focused on either blocking coinhibitory
62 receptor-ligand interactions or activating co-stimulatory receptor-ligand pathways. Despite
63 these advances, our understanding of the functions and regulatory mechanisms of these co-
64 signaling receptors remains incomplete. One such notable pathway is the one initiated by the
65 interaction of CD2 receptor on T cells and CD58 ligand on target cells, which has garnered
66 significant attention recently[2,3]. Patricia Ho *et al*[2]. and Beiping M. *et al*.[4,5] identified CMTM6 as
67 a positive regulator of CD58 in tumour cells. They found that competition for this regulator
68 between CD58 and the coinhibitory ligand PD-L1, which binds to PD-1, plays a critical role in
69 shaping downstream T cell anti-tumor responses.

70 We and others have demonstrated that peripheral blood CD4+ and CD8+ memory T cell
71 subsets express higher levels of CD2 compared to their naïve counterparts[4,5]. We recently
72 determined that the expression levels of CD2 on T cells influence the extent of CD2-CD58
73 interactions during T cell synapse formation[5]. These interactions, in turn, significantly amplify
74 proximal T cell receptor (TCR) signaling. Furthermore, we observed that strong PD-1
75 signaling—characterized by elevated PD-1 expression akin to that found in tumor-infiltrating T
76 cells (TI-T cells)—partially inhibits the CD2-mediated enhancement of proximal TCR signaling.
77 Notably, in a significant percentage of patients with colorectal (CRC), endometrial (EndoC),
78 and ovarian cancers (OC), we detected a tumour infiltrating (TI) CD8+ T cell population with
79 significantly reduced CD2 expression, which we termed the $CD2^{low}$ phenotype.

80 TI-T cells are frequently described as exhausted due to chronic antigen stimulation,
81 characterized by a progressive loss of effector functions[6,7]. The previously recognized pool of
82 exhausted TI-T cells has been further classified into progenitor exhausted (Tpex), transitory,
83 and terminally exhausted (Tex) T cells[8,9]. This classification reflects their potential
84 differentiation trajectory, with Tpex maintaining greater stemness properties than Tex cells,
85 such as self-renewal, long-term maintenance and effector exhausted T cells capable of
86 efficient tumour clearance. A Tpex signature has been associated with improved responses to
87 immune checkpoint blockade and enhanced efficacy of adoptively transferred T cells against
88 cancer[10–13]

89 Here, we employed ex vivo profiling of human T cells, in vitro functional assays, and genetic
90 screening approaches to deepen our understanding of CD2 function and regulation. We
91 determined that varying strengths of CD2 costimulation significantly affect downstream T cell
92 proliferation and IFN-γ production. Additionally, we found that the $CD2^{low}$ phenotype is also
93 exhibited by glioblastoma and meningioma CD4+ TI-T cells alongside CD8+ T cells. In our
94 quest to identify positive regulators of CD2 expression, we discovered that BRCA-1 associated

protein 1 (BAP1) is essential for expressing and maintaining high levels of CD2 expression in T cells; moreover, we determined that BAP1 serves as a broader regulator of key co-signaling receptors involved in T cell function other than CD2 and factors regulating T cell stemness, and metabolism.

RESULTS

T cell proliferation and IFN-γ production correlate with CD2 costimulation strength.

We previously demonstrated that interactions between CD2 and CD58 in the T cell synapse linearly amplify proximal T cell receptor (TCR) signaling. To investigate how the strength of CD2 costimulation affects downstream T cell responses, we monitored the proliferation of CFSE-labeled human peripheral blood (PB) naïve and memory T cells after polyclonal in vitro activation, with varying levels of CD2 costimulation and interleukin-2 (IL-2) cytokine. We observed that decreasing CD2 costimulation levels resulted in reduced percentages of proliferating cells, as shown in Fig. S1a-b. Focusing on the proliferating cells, we found that lower CD2 costimulation led to a significant decrease in both the average number of cell divisions and the fold expansion of these cells, as indicated by the proliferation index (PI) and replication index (RI), respectively; this trend was consistent across both PB CD4+ and CD8+ T cell compartments (Fig. 1a-b, S1c-d). Notably, PI and RI positively correlated with IL-2 receptor alpha (CD25) expression measured two days post-activation (Fig. 1c-d, S1e), suggesting that the strength of CD2 costimulation may regulate T cell proliferation following activation and IL-2 stimulation by modulating CD25 expression. A similar pattern was observed for IFN-γ production in an in vitro differentiation setting of naïve CD4+ T cells into Th1 cells. The effect mediated by CD2 was particularly pronounced for IFN-γ compared to IL-2 T cell production. A decrease in CD2 costimulation resulted in both a reduced percentage of IFN-γ-producing T cells and a lower level of IFN-γ produced by these cells, as illustrated by changes in high, intermediate, and low IFN-γ producers (Fig. 1e, S1f).

A $CD2^{low}$ phenotype exhibited by brain tumour-infiltrating CD8+ and CD4+ T cells.

We previously demonstrated that the expression levels of CD2 on T cells can limit CD2 costimulation, with PB memory T cells exhibiting a higher number of CD2 molecules compared to naïve T cells[5]. Building on these findings, we compared CD2 expression levels in T cells infiltrating human glioblastoma and meningioma (gli T and mng T cells) with their peripheral blood (PB) T cell counterparts. By categorizing PB, mng, and gli T cells using naïve and memory markers (CD62L and CD45RA) (Fig S2a), we observed reduced CD2 expression in both gli T and mng T cells within each memory-marker expressing (central memory, CM, effector memory, EM and EM re-expressing CD45RA, EMRA) CD8+ T cell compartment (Fig. 2a,c). Notably, this reduction aligned their CD2 expression more closely with that of corresponding naïve PB T cells across all patients; naïve T cells were almost completely absent from these tumours (Fig. S2a). This phenomenon is reminiscent of the $CD2^{low}$ phenotype we previously described in colorectal (CRC), endometrial (EndoC) and ovarian cancer (OC) patients. In contrast to our earlier studies in CRC, EndoC, and OC cohorts, the

145 CD2^{low} phenotype was also evident and strong in the tumor CD4+ T cell compartment for
146 nearly all brain cancer patients (Fig. 2b-d). Our findings, expand our initial observation from
147 other cancer types to brain tumours and reveal a unique difference in that the CD2^{low}
148 phenotype is also exhibited by in gli and mng CD4+ T cells and not just gli and mng CD8+ T
149 cells. This is important to consider since it has been shown that activation of both subsets is
150 required for functional anti-tumour T cell immunity in brain tumours[14–16]
151
152 **Genome-scale CRISPR-Cas9 screen identifies positive regulators of CD2.**
153 In light of the differential CD2 expression levels detected in the various T cell subsets, we
154 sought to identify regulators of CD2. We performed a positive selection, using fluorescence-
155 activated cell sorting (FACS), genome-wide CRISPR-Cas9 loss-of-function (LOF) screen in
156 Jurkat T cells (Fig. 3a). Perturbations enriched in the positively selected T cell population with
157 low CD2 surface protein (CD2lo) could be physiological positive regulators of CD2. Six targets
158 were consistently enriched across different time points in the CD2lo T cell population
159 compared to the control group, with CD2 itself being the most frequently identified target. (Fig.
160 3b-c, Supplementary Table 1). The nuclear deubiquitinating enzyme BRCA1-associated
161 protein-1 (*BAP1*) that was shown to be essential for thymocyte development and proliferative
162 responses of T cells, was the next most frequently enriched target after *CD2* hence our focus
163 thereafter. Amongst the six enriched targets, there was another epigenetic regulator gene the
164 SUZ12 polycomb repressive complex 2 (PRC2) subunit that forms part of the PRC2 repressive
165 complex. Subsequent experiments involving independent BAP1 gene and SUZ12 knockouts
166 (Kos) confirmed that BAP1 and SUZ12 regulate CD2 expression with the strongest effect seen
167 upon BAP1 KO relative to SUZ12 loss (Fig. 4 d-f). Real-time qPCR indicated a reduction in
168 *CD2* mRNA upon BAP1 or SUZ12 KO suggesting that they may exert their regulatory effect
169 at the transcriptional level (Fig. 4g).
170
171 **CD2 expression is co-regulated with expression of markers associated with T cell**
172 **development, stemness, exhaustion and metabolism.**
173 To investigate whether BAP1 KO affects only CD2 expression expression, we conducted a
174 bulk transcriptomic analysis comparing BAP1 KO Jurkat T cells to wild-type (WT) Jurkat T
175 cells. BAP1 KO led to the identification of 2107 differentially expressed genes (DEGs) relative
176 to the WT (Fig. 4a, log2FC > 0 and adjusted P-value < 0.05), with 1026 genes being
177 upregulated and 1081 downregulated (Supplementary Table 2a). This altered transcriptional
178 profile following BAP1 KO was characterized by the downregulation of key T cell surface
179 receptors, beyond that of *CD2,* notably *CD28* and *CD226* with *TRAC* being amongst the top
180 10 DEGs, and the upregulation of others such as *CD3G*, *CD3E*, *TNFRSF4/OX40*, *PTCRA*,
181 and *CD81* (Fig. 4b). Changes in total TRAC protein levels were validated using western

182 blotting (Fig. S3a) and the loss of TCR complex at the cell surface and other surface receptors
183 was confirmed using flow cytometry (Fig. S3b). Downregulated genes included molecules
184 involved in adhesion and cell trafficking (*SELL*, *ITGA1*, *ITGA4*, *ITGAL*, *ICAM2*, *ALCAM*) (Fig
185 4b). These results indicate BAP1 regulation is not specific to CD2 but affects additional
186 essential receptors involved in T cell development, T cell identity and migration. BAP1 KO
187 resulted in alterations in genes regulating T cell differentiation such as RORA, GATA3, PTPA
188 and solute transporters regulating metabolism such as GLUT1, GLUT3 (Fig. 4c). BAP1 KO
189 resulted in DEG associated with T cell stemness, differentiation to memory, progenitor
190 exhausted and exhausted T cells. Gene expression changes in group A genes (*TOX*, *TOX2*,
191 *TCF7*, *ID2*, *SNX9* etc) (Fig. 4c) would favour T cell stemness based on separate studies
192 investigating each individual gene independently. In contrast, gene expression changes in
193 Group B genes (*ACSS2, ID3*, *MYB*, *PRKCQ*, *PRKCH*, *LMO4* etc) have been associated with
194 reduced T cell stemness and would favour a T cell exhaustion state. TOX2 has been attributed
195 contrasting roles with potentially context-dependent differences i.e. its expression imposes T
196 cell exhaustion[17] or promotes central memory differentiation and prevents exhaustion in a
197 context dependent manner[18]. Interestingly, there was an increase in CD57+ T cells upon BAP1
198 KO CD57 expression and a 1.4-1.7-fold increase in CD57 average expression amongst
199 CD57+ T cells compared to WT ones (Fig S4c). This is suggestive of increased terminal
200 differentiation phenotype upon BAP1 loss as CD57 expression has been associated with
201 terminally differentiated CD8+ T cells[19] and T cell senescence[20] but also with the responding
202 T cells to anti-PD-1 checkpoint therapy in non-small cell lung cancer[21,22].
203 Gene ontology analysis (Fig. 4d-e, Suppl, Fig. 3c, Supplementary Table 2b-c) confirmed
204 BAP1's role in regulating genes involved in T cell receptor signaling regulation, T cell synapse,
205 adhesion processes, T cell differentiation, immune system development and metabolism such
206 as glucose metabolism, and insulin response. It further revealed involvement of BAP1 in
207 regulating genes involved oxidative phosphorylation, regulation of telomeres and post-
208 translational protein modification pathways. KEGG analysis, revealed enrichment of pathways
209 associated with cell cycle, Notch, TGF-beta and FoxO signaling pathways, nucleotide and fatty
210 acid metabolism and finally oxidative phosphorylation and cellular senescence (Fig. 4e,
211 Supplementary Table 2d).
212 Similar to the transcriptomic data findings, gene set enrichment analysis (GSEA) indicated a
213 downregulation of processes related to immune responses, T cell activation and
214 differentiation. In contrast, there was an upregulation of processes associated with ribosome
215 biogenesis, non-coding RNA processing and metabolic processes (Fig. 4f, Supplementary
216 Table 2e). GSEA also indicated similarities between BAP1 KO-induced gene changes and
217 those observed in human intrathymic T progenitor cells compared to CD4 thymocytes,
218 suggesting a role of BAP1 in thymocyte development. Additionally, parallers were drawn with

219 gene expression differences in HIV-specific CD8 T cells of HIV controllers compared to
220 progressors (Fig 4g, Supplementary Table 2f). Generating a Tpex gene signature by
221 comparing the DEGs of Tpex (CD101-Tim3- T cells), to Tex (CD101+Tim3+ T cells) from a
222 previous mouse study[8] and in the context of mouse-human orthologs, we run a GSEA on this
223 Tpex signature using our DEGs of BAP1KO T cells (Fig 4h). This revealed that BAP1KO T
224 cells downregulate a number of genes also downregulated in Tpex. At the same time, BAP1KO
225 T cells also downregulated genes that were found upregulated in Tpex. These findings,
226 although contrasting between them, they agree with our manual interpretation of our
227 transcriptomic findings (Fig. 4b) that show that upon BAP1 KO there are changes that can
228 both favour and disfavor an enhanced T cell stemness state. In summary, under our
229 experimental conditions CD2 was regulated together with a number of other costimulatory
230 receptors and stemness-, exhaustion- associated factors.
231
232 **BAP1 has dose-dependent effect on costimulatory receptor expression and stemness-**
233 **exhaustion transcription factors.**
234 Upon profiling T cells 7 days post sgRNA BAP1 transduction for BAP1 KO, we observed a
235 significant increase in the percentage of the CD3-CD2+ subset (Single Positive, SP) compared
236 to the control. Notably, it was not until 12 days post-transduction that a significant increase in
237 the CD3-CD2- (Double Negative, DN) subset, indicating loss of CD2, was detected; this subset
238 continued to rise over time, peaking around days 20 to 30 post-transduction (Fig. 5a and Fig.
239 S4a). The expression profile of CD3 and CD2 achieved by the end of the experiment was
240 maintained during further culturing of the T cells. Unexpectedly, BAP1 protein levels varied
241 among these subsets, decreasing from SP to DN (Fig. 5b), with the highest expression found
242 in the wild-type (WT) control, as expected. Similarly to the titrated levels of BAP1 observed in
243 the DN and SP subsets, there was a corresponding titrated effect on the surface expression
244 of co-stimulatory and adhesion receptors (Fig. 5c, Fig. S4b) shown to be downregulated at the
245 protein level and upon bulkRNAseq analysis; this was observed using two different sgRNAs
246 to KO BAP1 (Fig. 4b, Fig S4b). The DN subset exhibited the lowest levels of CD2, CD28,
247 CD11a, and CD49a, with expression levels increasing in the SP subset and the highest being
248 in the WT control; the same trend is observed in the percentage of positive cells for each
249 marker. Notably, CD58 expression did not show significant differences between these subsets
250 or compared to the WT control. A similar BAP1 dose-dependent effect on surface receptor
251 expression was observed for transcription factor genes related to T cell stemness *(tox, tcf1,*
252 *bach2, id2*) (Fig. 5d).
253
254

255 **T cell activation reveals differential CD2 and TCR expression in WT versus BAP1 KO T**
256 **cells but not for CD28 and CD226.**
257 CD2 expression is significantly upregulated following T cell activation. In DN BAP1KO T cells,
258 the expression of the TCR/CD3 complex was nearly absent. To activate both wild-type (WT)
259 and DN BAP1KO T cells, we employed phorbol myristate acetate (PMA) and/or ionomycin
260 (ION) treatment at low and high concentrations and in combinations, circumventing the need
261 for TCR/CD3 engagement. Activation was assessed through the expression of the activation
262 marker CD69, revealing that both T cell clones could be activated (<80% WT T cell activation)
263 but DN BAP1KO T cells exhibited compromised activation under ION-only stimulation
264 conditions. (Fig. S5a-b). CD2 expression was assessed two days after stimulation and again
265 at 11-12 days post-stimulation. As anticipated, WT Jurkat T cells exhibited a 1.8-fold increase
266 in average CD2 expression upon stimulation compared to resting conditions, with similar
267 increases observed for combinations of PMA with ION (1.2-1.8-fold) and high concentrations
268 of ionomycin alone (1.5-fold); nearly all WT T cells were CD2+ across all conditions. In
269 stimulated DN BAP1KO T cells, an upregulation of CD2 was detected, resulting in
270 approximately 21% CD2+ DN T cells compared to 5% CD2+ in resting conditions (Fig. 6a).
271 Despite this increase, CD2 levels in DN BAP1KO T cells remained significantly lower (about
272 8-fold less) than those found in resting WT T cells. Subsequent culture of T cell clones under
273 resting conditions led to a reduction in the percentage of CD2+ DN BAP1KO T cells, except
274 for those stimulated with high PMA concentrations, which maintained around 20% CD2+ DN
275 T cells (Fig 6b, Fig S5c). This trend in CD2 expression contrasted sharply with the behavior of
276 CD28 and CD226 upon stimulation followed by rest. While CD28 and CD226 were upregulated
277 in WT T cells, they also showed significant upregulation in DN T cells under PMA-containing
278 stimulations, reaching levels comparable to those in resting or activated WT T cells,
279 respectively. Phenotypic analysis following subsequent culturing in resting conditions, showed
280 that over 50% of DN T cells retained the upregulated CD28 or CD226 expression at levels
281 similar to those observed in WT T cells (Fig. 6b). WT T cells strongly upregulated the co-
282 inhibitory PD-1 receptor, upon high PMA-high ION stimulation (78% PD-1+ T cells) but DN
283 BAP1KO T cells showed significantly lower percentage of PD-1+ T cells (42% PD-1+ T cells),
284 despite similar levels of activation based on CD69 activation marker expression two days post-
285 activation (Fig. S5b,c). Within PD-1+ T cells, the average PD-1 expression was lower in PD-
286 1+ DN BAP1KO T cells (gMFI: 28851) compared to PD-1+ WT T cells (gMFI:70206). This
287 suggests that like CD2 expression, BAP1 is required for efficient and high expression of PD-
288 1 upon T cell activation. Finally, high ION with or without PMA stimulation resulted in increased
289 TCR expression in both WT and DN BAP1KO T cells relative to resting condition (Fig 6a, Fig
290 S5c). Despite this upregulation, DN BAP1KO T cells had a lower percentage of TCR+ T cells
291 compared to WT T cells; in fact, average TCR expression was half-fold lower in TCR+ DN

292 BAP1KO T cells compared to WT TCR+ T cells. Subsequent culturing in resting conditions
293 resulted in a decrease of TCR+ T cells in both T cell clones; this contraction, though, was more
294 pronounced in DN T cell population compared to WT T cells (Fig S5d-e). These findings reveal
295 differential mechanisms governing the expression of costimulatory receptors upon T cell
296 activation compared to resting conditions for distinct gene groups—namely CD2 and TCR
297 versus CD28 and CD226—highlighting the context-dependent nature of gene regulation.
298
299 **Pharmacological inhibition of histone deacetylases partially rescues BAP1 loss-**
300 **mediated CD2 repression.**
301 ATAC-seq analysis revealed that within and around the *CD2* locus there are condensed
302 regions of chromatin relative to WT; this is similar for the *TOX* locus. This suggests that loss
303 of BAP1 results in CD2 repression by through chromatin condensation that is one know way
304 of transcriptional regulation[23,24]. One such epigenetic mechanism driving this chromatin
305 condensation is the accumulation of tri-methylation of lysine 27 on histone H3 protein
306 (H3K27me3) carried out by the Polycomb repressive complex 2[24,25]. We treated DN BAP1KO
307 T cells with a number of PRC2 complex inhibitors (PRC2 catalytic subunit enhancer of zeste
308 homolog 2, EZH2, inhibitors) to see if this rescues the loss of CD2 but there was no
309 upregulation of CD2 (Fig. 7a, top). In contrast, EZH2 inhibitor treatment of WT cells resulted
310 in a dose-dependent reduction of CD2 expression (Fig. S7b), agreeing with our GW CRISPR-
311 Cas9 genetic screen that identified SUZ12 as a potential regulator of CD2 expression; SUZ12
312 is one of the members of the PRC2 complex together with EZH2. Repression of CD2
313 expression was confirmed in independent gene KOs of EZH2 (Fig. S7c). BAP1 KO has been
314 shown to not only increase global H3K27me3 but also reduce oH3K27acetylation (K3K27ac)
315 around gene promoters[26]. To investigate, whether counteracting loss of H3K27ac upon
316 BAP1KO upregulates CD2 expression, we treated DN BAP1KO T cells with the histone
317 deacetylase inhibitor, LMK235. This resulted in a partial rescue of CD2 loss upon BAP1 loss.
318 There was a dose-dependent upregulation of CD2 expression with increasing levels of the
319 HDAC inhibitor (Fig 7b); this upregulation though was not strong enough to reach the high
320 levels seen in WT T cells. These findings suggest there is an interplay between BAP1 activity
321 and HDAC activity in regulating CD2 expression. However, boosting H3K27ac is apparently
322 not enough on its own to enable high levels of CD2 expression in the absence of BAP1.
323
324
325
326
327
328

329 **DISCUSSION**

330 Through, this work, we identified novel regulatory properties of the CD2-CD58 costimulatory
331 pathway in human T cells; a pathway that has attracted significant interest in the fields of
332 cancer immunology and immunotherapy[2,3,5,27–29] over the past five years. Our findings reveal
333 that CD2 costimulation strength regulates downstream T cell responses and identify positive
334 regulators of CD2 expression, including the epigenetic regulators SUZ12 and BAP1. While
335 focusing on BAP1, which has been understudied in T cell biology, we demonstrated that BAP1
336 acts as a broader regulator of key co-stimulatory and co-inhibitory receptors, beyond CD2,
337 that are involved in T cell function and identity and it does so in a dose-dependent manner.
338 Additionally, BAP1 co-regulated genes associated with T cell stemness, exhaustion, and
339 metabolism.

340 We demonstrated that increasing CD2 costimulatory strength, not only enhances the
341 percentage of T cells that get activated but it increases the average number of divisions
342 (proliferation index, PI) and the fold expansion (replication index, RI) of these activated T cells.
343 Furthermore, increasing CD2 costimulation strength correlated with increasing expression of
344 the high affinity subunit of the IL-2 receptor, CD25, whose expression also shows a positive
345 correlation with PI and RI. These correlations suggest that CD2 costimulation strength may
346 regulate PI and RI by modulating CD25 expression levels, thereby influencing responses to
347 the proliferation-inducing IL-2 cytokine. We also observed a similar titration effect of CD2
348 costimulation strength on IFN-γ production in an *in vitro* Th1 differentiation context. This aligns
349 with a recent study showing that overexpression of CD58 in a melanoma cell line leads to
350 higher IFN-γ production in an in vitro T cell:tumour cell co-culture system[30].

351 Our results have significant implications for T cell anti-tumour immunity. We found that
352 human TI-T cells in glioblastoma and meningioma, despite of their expression of memory
353 markers, exhibit significantly reduced levels of CD2 resembling the levels observed in PB
354 naïve T cells. This observation is reminiscent of the $CD2^{low}$ phenotype we previously described
355 in CD8+ TI-T cells in a percentage of CRC, EndoC and OC patients[5]. Moreover, in these GBM
356 and MNG cohorts we also detected reduced CD2 expression in CD4+ TI-T cells in almost all
357 patients; this was not exhibited by CD4+ TI-T cells in our previously studied cancer types and
358 cohorts. This is important to consider since it has been shown that activation of both subsets
359 is required for functional anti-tumour T cell immunity in brain tumours[14–16] The reduction of
360 CD2 expression in TI- T cell may serve as an immune evasion mechanism imposed by the
361 tumour microenvironment, akin to the loss of CD58 observed in hematological
362 malignancies[31,32] . This phenomenon could indicate a poor prognosis or predict inadequate
363 responses to certain immunotherapies, similar to the lack of clinical benefit seen in melanoma
364 patients with low CD58 expression when treated with immune checkpoint blockade[2]. In fact,
365 in a recently published partially-humanised melanoma model study[2], it has been shown that

366 the absence of CD58 expression in tumour cells compromises T cell tumour infiltration,
367 activation and cytotoxicity, similar to an earlier *in vitro* cytotoxicity screen[33], further highlighting
368 the potential impact reduced CD2 costimulation strength could have on human anti-tumour T
369 cell immunity.

370 Through a genome-wide CRISPR-Cas9 KO screen, we report novel findings of genetic
371 regulators of CD2 expression. We identified the epigenetic regulators SUZ12 and BAP1 as
372 two positive regulators of CD2 expression. Focusing on BAP1 - given its limited
373 characterization in T cells - and employing bulk RNA sequencing analysis, flow cytometry,
374 gene ontology and GSE analyses, we determined that BAP1 acts as a broad regulator of gene
375 expression in T cells. BAP1 KO affected the expression of a number of groups of genes
376 including co-stimulatory/inhibitory receptors, beyond CD2, adhesion molecules, transcription
377 factors involved in T cell development and differentiation, factors involved in the balance
378 between T cell stemness and exhaustion and genes regulating cell metabolism. This agrees
379 with the role of BAP1 described in other cell types especially in cancer cells as a regulator of
380 gene expression by constraining ubiquitination of genome histones[34 35]. We also show that
381 BAP1 has a dose-dependent effect on the regulation of costimulatory receptors and stemness-
382 exhaustion-associated factors. BAP1 overexpression studies such as this[36] might have hinted
383 on this dose-dependent effect before. Notably, BAP1 KO T cells exhibited a mixed phenotype
384 characterized by enriched stemness and exhaustion markers. Further investigation is
385 warranted to elucidate how the BAP1 KO-mediated expression changes in stemness- or
386 exhaustion-associated factors influence downstream T cell anti-tumour immunity in vivo.
387 Interestingly, a very recent study[37] using a mouse chronic infection model and ASXL1 KO P14
388 T cells – ASXL1 is a key partner of BAP1 in the Polycomb repressive deubiquitinase complex,
389 PR-DUB [38,39]– showed that although ASXL1 KO T cells had higher frequency of Tex compared
390 to WT T cells, bulk RNA sequencing of ASXL1 KO T cells showed lower expression of TOX, a
391 Tex associated marker, in ASXL1 KO T cells and higher expression of Tpex associated genes
392 such as *Tcf7* and *Myb*. Considering their findings and mechanistic insight describing that
393 ASXL1 KO results in reduced activity of the PR-DUB complex, one might suggest that human
394 BAP1 KO T cells might show a similar phenotype in an *in vivo* cancer setting but this is yet to
395 be confirmed. However, a mouse study[40] comparing BAP1 KO and ASXL1 KO tumour cells
396 revealed significant similarities and differences in the genes regulated in each KO so one
397 should take caution in extrapolations; the degree of similarity between the two KO phenotypes
398 could be cell- and/or context-specific. Our transcriptomic findings showing that BAP1 regulates
399 key factors involved in T cell development including the *TRAC* and pre-TCRA (*PTCRA*) and
400 our GSEA findings that BAP1 KO has an enriched gene signature for genes downregulated in
401 thymic T cell progenitors agree with the first study[41] investigating mouse BAP1 KO T cells; it

402 showed defective thymocyte development, impaired T cell proliferation in mature T cells in the
403 periphery and impaired Th17 differentiation upon BAP1 KO.
404 Finally, we showed that BAP1 is essential for efficient high expression of CD2 upon T
405 cell activation as CD2 was only partially upregulated and sustained upon T cell chemical
406 activation in contrast to CD28 and CD226 that showed high and sustained expression. This
407 suggests that T cell activation induces pathways that can rescue loss of CD28 and CD226
408 due to BAP1 KO, but these are not sufficient to restore CD2 expression. It is yet to be
409 determined what are these exact pathways. CD2 expression though was rescued in BAP1 KO
410 T cells by inhibiting histone deacetylases. A similar pharmacological rescue of a BAP1 KO
411 phenotype was observed for the gastrulation process during embryo development of *Xenopus*
412 *laevis*[26] . We suggest that this is the result of increasing histone acetylation that allows a more
413 open chromatin structure[42,43] counteracting the closer chromatin at the CD2 locus induced by
414 BAP1 KO as shown by our ATAC-Seq analysis.
415 In summary, our work has contributed to three major advances in T cell biology. First,
416 we elucidate a previously unappreciated role of CD2 costimulation strength in downstream T
417 cell responses further boosting our suggestion that the $CD2^{low}$ phenotype, now also described
418 in glioblastoma and meningioma T cells, is another pathway impacting anti-tumour T cell
419 immunity. Second, we identify positive regulators of CD2 expression including two epigenetic
420 regulators, SUZ12 and BAP1. Finally, we demonstrate that under steady state conditions CD2
421 is co-regulated by BAP1 with other costimulatory receptors and stemness- and exhaustion-
422 associated factors further highlighting the link of the CD2 pathway with other key pathways
423 determining T cell responses in diseases such as cancer.
424
425
426
427
428
429
430
431

MATERIALS AND METHODS

Reagents

RPMI-1640 (31870074), Fetal Bovine Serum (FBS), Phosphate-buffered saline (PBS) and Dynabeads Human T-Activator CD3/ CD28 for T cell expansion and Activation kit (1132D) were purchased from Thermo Fisher Scientific. The following anti-human antibodies were purchased from Biolegend: CD62L (DREG-56), CCR7 (G043H7), CD3 (SK7), CD4 (SK3), CD8 (RPA-T8), CD28 (CD28.2), PD-1 (EH12.2H7), mouse IgG1 isotype control (MOPC-21), Human TruStain FcX, CD45 (HI30), CD45RA (HI100), CD2 (RPA2.10), CD57 (QA17A04), CD96 (NK92.39), CD11 (HI111), TCR-αβ (IP26), CD226 (11A8), CD127 (A019D5), CD49a (TS2/7), CD58 (TS2/9), CD3 (OKT3), CD69 (FN50), CD25 (M-A251). The following antibodies were purchased from Cell Signalling: BAP1 (D7W7O), CD3ε (D7A6E), TRBC1/TCRβ constant region 1 (E6Z3S), GAPDH (D4C6R), β-actin (8H10D10). The following antibody was purchased from Santa Cruz Biotechnology: TCR α Antibody (H-1). The following antibody was purchased from Proteintech: CD2 Monoclonal antibody (3A10B2). The following Taqman primer-probes were purchased from Thermo Fisher Scientific: Bap1 (Hs00184962_m1), Cd2 (Hs01040180_m1), Abl 1 (Hs01104728_m1), Tox (Hs01049519_m1), Tcf7 (Hs01556515_m1), Bach2 (Hs00935338), Id2 (Hs04187239). Antibodies were used at dilutions recommended by the manufacturer for western blotting and at concentrations in the range of 0.5-2 μg/ml for flow cytometry depending on the titration experiments and number of cells stained. The BlueStar Prestained Protein Marker (MWP03) was purchased from Nippon Genetics.

Isolation of PBMCs and T cells from human samples

Human PBMCs and T cells were isolated from leukapheresis products of healthy controls (Cyprus National Bioethics Committee License 2020/44) or fresh peripheral blood of cancer patients (Cyprus National Bioethics Committee License 2020/45) using Ficoll-Paque density gradient as per suppliers instructions followed by an erythrocyte lysis step using ACK lysis buffer (ThermoFisher A1049201) as per manufacture's protocol; T cell subsets were isolated using negative selection EasySep enrichment kits from STEM CELL Technologies. T cells were maintained when necessary in resting conditions, in the absence of any IL-2, at 37°C, 5% CO2, in RPMI medium (Life Technologies) supplemented with 10% FBS, 5% Penicillin-Streptomycin, (Penstrep, Gibco), 1x MEM Non-Essential Amino Acids Solution (Thermo Fisher Scientific), 10mM HEPES (Life Technologies), 1mM Sodium Pyruvate (Thermo Fisher Scientific). T cells were maintained at maximum $2x10^6$ cells/ml for a maximum of 5 days during resting conditions.

469 **Single cell suspensions of human brain tumour samples**

470 Preparation of single cell suspensions from fresh brain tumor tissue (BT) was carried out as
471 described previously in[44]. In brief, the sample was cut into small fragments (approximately 1–
472 2 mm^3) and resuspended in Hanks' Balanced Salt solution ($HBSS^{(+Ca+Mg)}$; Sigma-Aldrich, cat.
473 No. 55037C) at 100 mg tissue per ml. Then neutral protease (NP, AMSBio. S3030112) at 0.11
474 DMC U/ml and a Bovine pancreatic deoxyribonuclease I was used at 400U/ml (DNase I;
475 Sigma-Aldrich, 11284932001) were added to the suspension and incubated for an average
476 time of 2 hours at 37°C. The preparation was then filtered through a 70 µm strainer to remove
477 clumps. The single cell suspension was then washed once and resuspended in phosphate-
478 buffered saline (PBS, Fisher Scientific, 10010056) supplemented with 10% fetal bovine serum
479 (FBS, ThermoFisher, A5256801). The standard trypan blue dye-exclusion method was used
480 to evaluate cellular viability.

481

482 **Cancer patient cohort**

483 Sixteen fresh tumour samples from two sides of the tumour and matched peripheral blood in
484 EDTA-blood collection tubes from consented GBM and MNG patients were obtained from
485 patients who underwent surgical removal of tumours at the Aretaieio Private Hospital (Nicosia,
486 Cyprus). They were processed to generate single cell suspensions. Information about the age
487 and gender of the patients is shown in Supplementary Table 3.

488

489 **Human primary T cell activation and proliferation assays**

490 Proliferation of human T cells was monitored by following dilution of CFSE(Sigma-Aldrich)-
491 labelled T cells (Sigma-Aldrich). Briefly, T cells single cell suspensions at $3x10^6$ cells/ml in PBS
492 were stained with 1 µM CFSE in PBS solution by a 10 min incubation in a culture incubate at
493 37°C, 5% CO_2. Staining was quenched by adding FBS at a final 10% FBS concentration before
494 pelleting the cells to removed supernatant. Cells were washed and resuspended in culture
495 medium for downstream assays.Typically, T cells were prepared for T cell activation in U-
496 bottom plates at $1x10^6$/ml and activated with anti-CD3/CD28 antibody coated Dynabeads for
497 2 days before removing the activation stimulations and supplementing the culture with 30U/ml
498 IL-2. The culture was split every other day starting from the day of stimuli removal. At the
499 endpoint, T cells were stained with fixable viability ef780 dye (ThermoFisher) followed by a
500 mixture of fluorophore-conjugated antibodies when needed. Stained sampels were acquired
501 on a 3-laser Aurora spectral flow cytometer (Cytek)

502

503 **Profiling human samples using flow cytometry**

504 Human primary T cells, PBMCs, Jurkat T cells and cancer patient tumour single cell
505 preparations were stained at around $0.05x10^6$, $0.01x10^6$, $0.1x10^6$ and $1x10^6$ per staining

506 condition respectively in U-bottom plates. For PBMCs and cancer tumour samples an Fc-
507 receptor blocking step was carried out by resuspending cells in 50 µL PBS with 0.5% BSA and
508 5 µL Human TruStain FcX (BioLegend) per sample, followed by incubation at room
509 temperature for 10 minutes. Cells were stained with an antibody mix prepared in ice-cold
510 PBS/0.5% BSA and incubated on ice in the dark for 20 minutes. Antibodies were used in the
511 range of 0.5–2.5 µg/mL, based on the determined staining index of each antibody. Following
512 the antibody staining, the cells were washed twice in PBS/0.5%BSA and acquired on a 3-laser
513 Aurora flow cytometer. Data analysis was performed using FlowJo software (v10.8.1).
514
515 **In vitro differentiation of human naïve CD4+ T cells to Th1**
516 Human naïve CD4+ T cells were isolated as described above. They were activated for 2 days
517 using anti-CD3-CD28 antibody coated Dynabeads. The culture medium was supplemented
518 with a cytokine-containing cocktail supplemented also with cytokine blocking antibodies from
519 STEMCELL Technologies (ImmunoCult Human Th1 Differentiation Supplement, 10973)
520 recommended for differentiation to Th1; it was used at 1 in 500 dilution. Following removal of
521 activation beads, cells were split 1 in 2 every other day. Th1 status was profiled 7 days post-
522 initiation of experiment using intracellular cytokine staining for IL-2 and IFN-γ. Intracellular
523 cytokine staining was performed using the Foxp3 staining kit from eBioscience as per
524 company's instruction for a U-bottom two-step protocol.
525
526 **Genome wide (GW) CRISPR-Cas9 Knockout screen in Jurkat T cell line.**
527 For generation of constitutively Cas9-expressing cell lines, vector pKLV2-EF1a-Cas9Bsd-W
528 was packaged into lentivirus by co-transfection of HEK293T cells alongside lentiviral envelope
529 and packaging plasmids pMD2.G and psPAX2 using Lipofectamine LTX with PLUS reagent
530 (Invitrogen) as described in[45] . The Jurkat cell line was transduced with lentivirus carrying Cas9
531 in the presence of polybrene (8 µg/ml). The following day, lentiviral containing medium was
532 replaced with complete medium. Blasticidin selection was started on day 4 post transduction
533 at 4 µg/ml. Cas9 activity was assessed using a lentiviral reporter system consisting of the
534 constructs pKLV2-U6gRNA(gGFP)-PGKBFP2AGFP-W and pKLV2-U6gRNA(gEmpty)-
535 PGKBFP2AGFP-W. Cells were transduced with a predetermined viral amount of the genome
536 wide gRNA-BFP library that allows for an average of 30% transduction, measured by BFP
537 expression by cytometry and ensures incorporation of a sgRNA per cell with about 9% error
538 rate. Transduction was performed at 1×10^6 cells per well in 6-well plates for a total of 100×10^6
539 to allow for a 350x coverage of the library. Puromycin selection was used, starting at day 4 of
540 the culture, to select for cells that had successful lentiviral plasmid integration. Cell
541 transduction efficiency was determined before and after puromycin selection by quantifying
542 the percentage of BFP expressing cells using flow cytometry. FACSorting was performed at 5

543 different timepoints during cell culture of these cells, sorting for 5% of CD2low/neg cells from
544 the live T cell population. FACSorted T cells were stored in RNAlater in -20ºC till DNA
545 extraction, DNA library preparation and next-generation sequencing. The bioinformatic
546 analysis was performed as described previously in[44,46] using the MaGeCK package.
547

548 **Designing single guide RNAs(sgRNA) for sgRNA knock outs in T cells**

549 sgRNAs were designed using the CHOPCHOP and Synthego web tool or using the gRNA list
550 from the Human genome-wide lentiviral CRISPR gRNA library version 1(Addgene 67989)
551 (Supplementary Table 4). Priority was given to plasmids found enriched in the MaGeCK
552 analysis results of our screen. For online tools, selection criteria also included GC content
553 (>45%), efficiency score (>0.5), and minimal self-complementarity/mismatch scores.

554 **Western blotting**

555 Whole cell lysates were prepared by incubation of the cell pellet for 30 mins in 1X RIPA buffer
556 (Sigma-Aldrich, R0278) supplemented with 1 mM PMSF and 1X protease inhibitor cocktail
557 (Sigma-Aldrich, 11836153001) on ice. Supernatant was harvested and stored in -20°C till
558 required for downstream analysis. Total protein concentration was determined using the
559 Bradford assay. 50–100 µg of total protein was loaded per well in a 8 or 10% SDS-PAGE gel
560 depending on the molecular weight of the proteins of interest. Whole cell lysates were
561 prepared using 1X Laemmli loading buffer (Bio-Rad, 1610747) and denatured for 5 mins at
562 95°C. Proteins were transferred to Porablot nitrocellulose membranes (Macherey-Nagel,
563 741280) using a wet transfer system. Membranes were blocked in 5% nonfat milk or BSA
564 prepared in in TBS-T (Tris-buffered saline supplemented with 0.05% Tween-20) for 1 hour at
565 room temperature and incubated overnight at 4 °C with primary antibodies prepared in TBS-T
566 supplanted with 5%BSA or milk as per manufacturer's recommendations. After washing with
567 TBS-T, membranes were incubated with a IRD680RD or IRD800CW-conjugated secondary
568 antibody for 1 hour at room temperature. Following extensive washing, protein bands were
569 imaged on the Vilber imaging system. Protein band total intensities were quantified using FIJI
570 software, normalized to housekeeping proteins (β-actin or GAPDH) and presented as relative
571 protein expression.
572

573 **RNA extraction, real-time quantitative PCR, bulk RNA sequencing and differential**
574 **expression gene analyses.**

575 Total RNA was extracted using the MagCore® triXact RNA Kit (Cat.no. 631) as per
576 manufacturer's recommendations and assessed for quality and quantity using a NanoDrop™
577 2000/2000c Spectrophotometer. The RNA aliquots were stored at −80°C.

578 For real-time quantitative PCR (RT-qPCR), total RNA from each sample was used to
579 synthesize cDNA using PrimeScript RT Reagent Kit(Takara, cat. No RR037A) according to the
580 manufacturer's protocol. The reagents, RNA, oligo (dT), and dNTPs were mixed first, then
581 incubated at 37 °C for 15 mins, 85 °C for 5 mins and then chilled on ice. The samples were
582 stored at -20°C till required for downstream assays. RT-qPCR was performed using the
583 TaqMan™ Universal PCR Master Mix (Thermo Fisher Scientific, 4304437) for precise
584 quantification of gene expression. TaqMan primer-FAM probe pairs were purchased from
585 Thermo Fisher Scientific and are included in the reagents section above. The internal control
586 gene used was *ABL1* (Hs01104728_m1), and target genes used can be found in the reagents
587 paragraph. All of the reactions were run in triplicates on a CFX 96 (BioRad) thermal cycler.
588 The Cq values were estimated by analysing the data as a single pool, using the automatic
589 threshold and baseline cycle option of the CFX Manager Software v3.1. Amplifications were
590 conducted in triplicates on a real-time PCR system under the following thermal cycling
591 conditions: an initial step at 50 °C for 2 minutes, 95 °C for 10 minutes, followed by 50 cycles
592 of 95 °C for 15 seconds and 60 °C for 1 minute. Fluorescence was monitored throughout
593 amplification. Relative gene expression levels were calculated using the $2^{-\Delta\Delta CT}$ method,
594 normalized to *ABL1.*
595 cDNA libraries for bulk RNAsequening analysis were prepared from the extracted total RNA
596 using the QuantSeq 3'mRNA-Seq V2 Library Prep Kit-FWD (Lexogen; 192.96) according to
597 the manufacturer's guidelines. Three biological replicates of each sample were analyzed. The
598 pooled libraries were sequenced on an Illumina the NextSeq2000 system. Different expression
599 gene analysis was performed by the Lexogen pipeline using DESeq2 algorithm as described
600 on the company's website.
601
602 **Bioinformatic analysis including gene ontology, KEGG and Gene Set Enrichment**
603 **Analyses**
604 Bioinformatics analysis of differential expression findings was performed by utilizing the R
605 package clusterProfiler for functional enrichment analysis. Gene Ontology (GO) and Kyoto
606 Encyclopedia of Genes and Genomes (KEGG) enrichment analyses were conducted to
607 identify over-represented biological themes. Additionally, Gene Set Enrichment Analysis
608 (GSEA) was performed using gene sets from the Molecular Signatures Database (MSigDB)
609 collections C5 (ontology gene sets) and C7 (immunologic gene sets). All analyses were
610 conducted using default parameters within the respective functions. For the generation of a
611 Tpex signature, we utilised bulk RNAseq data from [8] and comparison of CD101-TIM-3- T cells
612 and CD101+TIM-3+ using the DESeq2 software package; differentially expessed genes with
613 a padj<0.05 and log2fold change>0 were used as a Tpex gene signature against which a
614 GSEA was performed with the DEG of BAP1 KO Jurkat T cells.

615 **Assay for Transposase-Accessible Chromatin using sequencing (ATAC-Seq) analysis.**
616 ATAC-seq analysis was performed using commercially available kit (Activemotif, 53150,) for
617 cell processing and library preparation. In brief, 50,000 cells were processed using the above
618 kit with one deviation of the incubation time required for the Tn5-mediated tagmentation of the
619 DNA that was extended to 1 hr instead of 30 mins as recommended in the manual of the kit.
620 Sample quality was assessed on an Agilent DNA tapestation using an Agilent D1000
621 screentape. Sequencing was performed on a NextSeq 2000 as per company's instructions
622 and analysis was performed by the the ATAC-seq analysis service of ActiveMotif company.
623
624 **Phorbol 12-myristate 12-acetate (PMA) and ionomycin treatment of T cells**
625 Wild Type (WT) or FACSorted CD3-CD2- (double negative, DN) Jurkat T cell subsets were
626 cultured in RPMI 1640 medium supplemented with 10% FBS, 2 mM L-glutamine, 100 IU/mL
627 penicillin, and 100 µg/mL streptomycin in a 37°C incubator with 5% CO_2 with or without
628 treatment with low levels of PMA (0.6ng/ml), high levels of PMA (20ng/ml) low levels of
629 Ionomycin (ION, 0.1µg/ml), high levels of ION, 1µg/ml or high levels of PMA combined to low
630 or high concentration of ION. Following two days of T cell treatment, culture media was
631 replaced and cells split every other day in fresh supplemented media in resting, no stimulation
632 conditions for an additional 9-10 days. T cell viability and expression of surface receptors was
633 evaluated 2 days post-stimulation and after 9-10 in resting culture conditions using flow
634 cytometry analysis.
635
636 **PRC2 and HDAC inhibitors treatment of Jurkat T cell subsets.**
637 Wild Type (WT) or FACSorted CD3-CD2- (double negative, DN) Jurkat T cell subsets were
638 cultured in supplemented RPMI 1640 medium with or without PRC2 complex inhibitors
639 (MedChemExpress, A-395, HY-101512; GSK126, HY-13470 ; Tazemetostat , Cat. No.: HY-
640 13803). Inhibitor treatment, at titrated concentrations, was started on day 0 and supplemented
641 on day 3 post-initiation of experiment. T cell viability and CD2 expression were evaluated 3
642 and 7 days post-initiation of experiment.
643
644 **Data analysis and statistics**
645 Data were analysed by GraphPad Prism v10 wherever needed unless mentioned otherwise
646 such as in the bioinformatics sections of bulk RNAseq analysis.
647

ACKNOWLEDGEMENTS

We wish to thank Dimitris Aspris for his assistance in transfering the knowledge on CRISPR-Cas9 genome wide screens in cell lines to CSHM, Skevi Charalampous and all the nursing staff of Aretaieio Hospital, Nicosia for helping out with the patient consents and sample acquisition, respectively.

Author contributions:

Conceptualisation:	PD,PC
Data curation:	PD, MI
	PD, MI, PC, DV, GG, VT, JC, VP,
Methodology:	SC
Investigation:	PD, MI, PC, DV
Funding acquisition:	PC, AA
Supervision:	PD, PC
Writing - original draft	PD, MI

Competing interests: Authors declare that they have no competing interests.

DATA AND MATERIALS AVAILABILITY: The data that support the findings of this study are available from the corresponding author upon reasonable request.

REFERENCES

1. Chen, L. & Flies, D. B. Molecular mechanisms of T cell co-stimulation and co-inhibition. *Nature Reviews Immunology* vol. 13 Preprint at https://doi.org/10.1038/nri3405 (2013).
2. Ho, P. *et al.* The CD58-CD2 axis is co-regulated with PD-L1 via CMTM6 and shapes anti-tumor immunity. *Cancer Cell* **41**, (2023).
3. Miao, B. *et al.* CMTM6 shapes antitumor T cell response through modulating protein expression of CD58 and PD-L1. *Cancer Cell* **41**, (2023).
4. Podestà, M. A. *et al.* Siplizumab selectively depletes effector memory T cells and promotes a relative expansion of alloreactive regulatory T cells in vitro. *American Journal of Transplantation* **20**, (2020).
5. Demetriou, P. *et al.* A dynamic CD2-rich compartment at the outer edge of the immunological synapse boosts and integrates signals. *Nat Immunol* **21**, (2020).
6. McLane, L. M., Abdel-Hakeem, M. S. & Wherry, E. J. CD8 T Cell Exhaustion During Chronic Viral Infection and Cancer. *Annual Review of Immunology* vol. 37 Preprint at https://doi.org/10.1146/annurev-immunol-041015-055318 (2019).
7. Kamphorst, A. O. *et al.* Rescue of exhausted CD8 T cells by PD-1-targeted therapies is CD28-dependent. *Science (1979)* **355**, (2017).
8. Hudson, W. H. *et al.* Proliferating Transitory T Cells with an Effector-like Transcriptional Signature Emerge from PD-1+ Stem-like CD8+ T Cells during Chronic Infection. *Immunity* **51**, (2019).
9. Rahim, M. K. *et al.* Dynamic CD8+ T cell responses to cancer immunotherapy in human regional lymph nodes are disrupted in metastatic lymph nodes. *Cell* **186**, (2023).
10. Miller, B. C. *et al.* Subsets of exhausted CD8+ T cells differentially mediate tumor control and respond to checkpoint blockade. *Nat Immunol* **20**, (2019).
11. Siddiqui, I. *et al.* Intratumoral Tcf1 + PD-1 + CD8 + T Cells with Stem-like Properties Promote Tumor Control in Response to Vaccination and Checkpoint Blockade Immunotherapy. *Immunity* **50**, (2019).
12. Mietz, J. *et al.* Human effector CD8+ T cells with an activated and exhausted-like phenotype control tumour growth in vivo in a humanized tumour model. *EBioMedicine* **106**, (2024).

13. Tabanelli, V. *et al.* The identification of TCF1+ progenitor exhausted T cells in THRLBCL may predict a better response to PD-1/PD-L1 blockade. *Blood Adv* **6**, 4634–4644 (2022).
14. Kilian, M. *et al.* MHC class II-restricted antigen presentation is required to prevent dysfunction of cytotoxic T cells by blood-borne myeloids in brain tumors. *Cancer Cell* **41**, (2023).
15. Mauldin, I. S. *et al.* Proliferating CD8+ T cell infiltrates are associated with improved survival in glioblastoma. *Cells* **10**, (2021).
16. Yang, I. *et al.* CD8+ T-cell infiltrate in newly diagnosed glioblastoma is associated with long-term survival. *Journal of Clinical Neuroscience* **17**, (2010).
17. Seo, H. *et al.* TOX and TOX2 transcription factors cooperate with NR4A transcription factors to impose CD8+ T cell exhaustion. *Proc Natl Acad Sci U S A* **116**, (2019).
18. Collins, S. M. *et al.* TOX2 coordinates with TET2 to positively regulate central memory differentiation in human CAR T cells. *Sci Adv* **9**, (2023).
19. Kared, H., Martelli, S., Ng, T. P., Pender, S. L. F. & Larbi, A. CD57 in human natural killer cells and T-lymphocytes. *Cancer Immunology, Immunotherapy* **65**, (2016).
20. Xu, W. & Larbi, A. Markers of T cell senescence in humans. *International Journal of Molecular Sciences* vol. 18 Preprint at https://doi.org/10.3390/ijms18081742 (2017).
21. Sun, W. *et al.* CD57-positive CD8 + T cells define the response to anti-programmed cell death protein-1 immunotherapy in patients with advanced non-small cell lung cancer. *NPJ Precis Oncol* **8**, (2024).
22. Huang, B. *et al.* CD8 + CD57 + T cells exhibit distinct features in human non-small cell lung cancer. *J Immunother Cancer* **8**, (2020).
23. Klemm, S. L., Shipony, Z. & Greenleaf, W. J. Chromatin accessibility and the regulatory epigenome. *Nature Reviews Genetics* vol. 20 Preprint at https://doi.org/10.1038/s41576-018-0089-8 (2019).
24. Margueron, R. & Reinberg, D. The Polycomb complex PRC2 and its mark in life. *Nature* vol. 469 343–349 Preprint at https://doi.org/10.1038/nature09784 (2011).
25. Yamagishi, M. *et al.* Mechanisms of action and resistance in histone methylation-targeted therapy. *Nature* **627**, (2024).

728 26. Kuznetsov, J. N. *et al.* BAP1 regulates epigenetic switch from pluripotency to
729 differentiation in developmental lineages giving rise to BAP1-mutant cancers. *Sci*
730 *Adv* **5**, (2019).
731 27. Romain, G. *et al.* Multidimensional single-cell analysis identifies a role for CD2-
732 CD58 interactions in clinical antitumor T cell responses. *Journal of Clinical*
733 *Investigation* **132**, (2022).
734 28. An, X. *et al.* EVOLVE205, a Highly Potent 2:1 CD20-Targeted CD2 Co-Stimulatory T
735 Cell Engager Engineered for the Treatment of B Cell Malignancies and B Cell
736 Autoimmune Diseases. *Blood* **144**, 2790–2790 (2024).
737 29. Jo, Y., Sim, H.-I., Yun, B., Park, Y. & Jin, H.-S. Revisiting T-cell adhesion molecules
738 as potential targets for cancer immunotherapy: CD226 and CD2. *Exp Mol Med*
739 (2024) doi:10.1038/s12276-024-01317-9.
740 30. Zurli, V. *et al.* Phosphoproteomics of CD2 signaling reveals AMPK-dependent
741 regulation of lytic granule polarization in cytotoxic T cells. *Sci Signal* **13**, (2020).
742 31. Archimbaud, E. *et al.* Expression of surface adhesion molecules CD54 (ICAM-1)
743 and CD58 (LFA-3) in adult acute leukemia: Relationship with initial characteristics
744 and prognosis. *Leukemia* **6**, (1992).
745 32. Abdul Razak, F. R., Diepstra, A., Visser, L. & Van Den Berg, A. CD58 mutations are
746 common in Hodgkin lymphoma cell lines and loss of CD58 expression in tumor
747 cells occurs in Hodgkin lymphoma patients who relapse. *Genes Immun* **17**,
748 (2016).
749 33. Patel, S. J. *et al.* Identification of essential genes for cancer immunotherapy.
750 *Nature* **548**, (2017).
751 34. Fursova, N. A. *et al.* BAP1 constrains pervasive H2AK119ub1 to control the
752 transcriptional potential of the genome. *Genes Dev* **35**, (2021).
753 35. Kwon, J., Lee, D. & Lee, S. A. BAP1 as a guardian of genome stability: implications
754 in human cancer. *Experimental and Molecular Medicine* vol. 55 Preprint at
755 https://doi.org/10.1038/s12276-023-00979-1 (2023).
756 36. Perez-Garcia, V. *et al.* Bap1/asxl complex modulation regulates epithelial-
757 mesenchymal transition during trophoblast differentiation and invasion. *Elife* **10**,
758 (2021).

759 37. Kang, T. G. *et al.* Epigenetic regulators of clonal hematopoiesis control CD8 T cell
760 stemness during immunotherapy. *Science (1979)* **386**, (2024).
761 38. Kolovos, P. *et al.* PR-DUB maintains the expression of critical genes through
762 FOXK1/2- A nd ASXL1/2/3-dependent recruitment to chromatin and H2AK119ub1
763 deubiquitination. *Genome Res* **30**, (2020).
764 39. Sahtoe, D. D., Van Dijk, W. J., Ekkebus, R., Ovaa, H. & Sixma, T. K. BAP1/ASXL1
765 recruitment and activation for H2A deubiquitination. *Nat Commun* **7**, (2016).
766 40. Lafave, L. M. *et al.* Loss of BAP1 function leads to EZH2-dependent
767 transformation. *Nat Med* **21**, (2015).
768 41. Arenzana, T. L. *et al.* Tumor suppressor BAP1 is essential for thymic development
769 and proliferative responses of T lymphocytes. *Sci Immunol* **3**, (2018).
770 42. Nitsch, S., Zorro Shahidian, L. & Schneider, R. Histone acylations and chromatin
771 dynamics: concepts, challenges, and links to metabolism. *EMBO Rep* **22**, (2021).
772 43. Chen, Y. J. C., Koutelou, E. & Dent, S. Y. R. Now open: Evolving insights to the roles
773 of lysine acetylation in chromatin organization and function. *Molecular Cell* vol.
774 82 Preprint at https://doi.org/10.1016/j.molcel.2021.12.004 (2022).
775 44. Volovitz, I. *et al.* A non-aggressive, highly efficient, enzymatic method for
776 dissociation of human brain-tumors and brain-tissues to viable single-cells. *BMC*
777 *Neurosci* **17**, (2016).
778 45. Tzelepis, K. *et al.* A CRISPR Dropout Screen Identifies Genetic Vulnerabilities and
779 Therapeutic Targets in Acute Myeloid Leukemia. *Cell Rep* **17**, (2016).
780 46. Li, W. *et al.* MAGeCK enables robust identification of essential genes from
781 genome-scale CRISPR/Cas9 knockout screens. *Genome Biol* **15**, (2014).
782
783
784
785
786
787
788
789

Fig 1. T cell proliferation and IFN-γ production correlate with CD2 costimulation strength

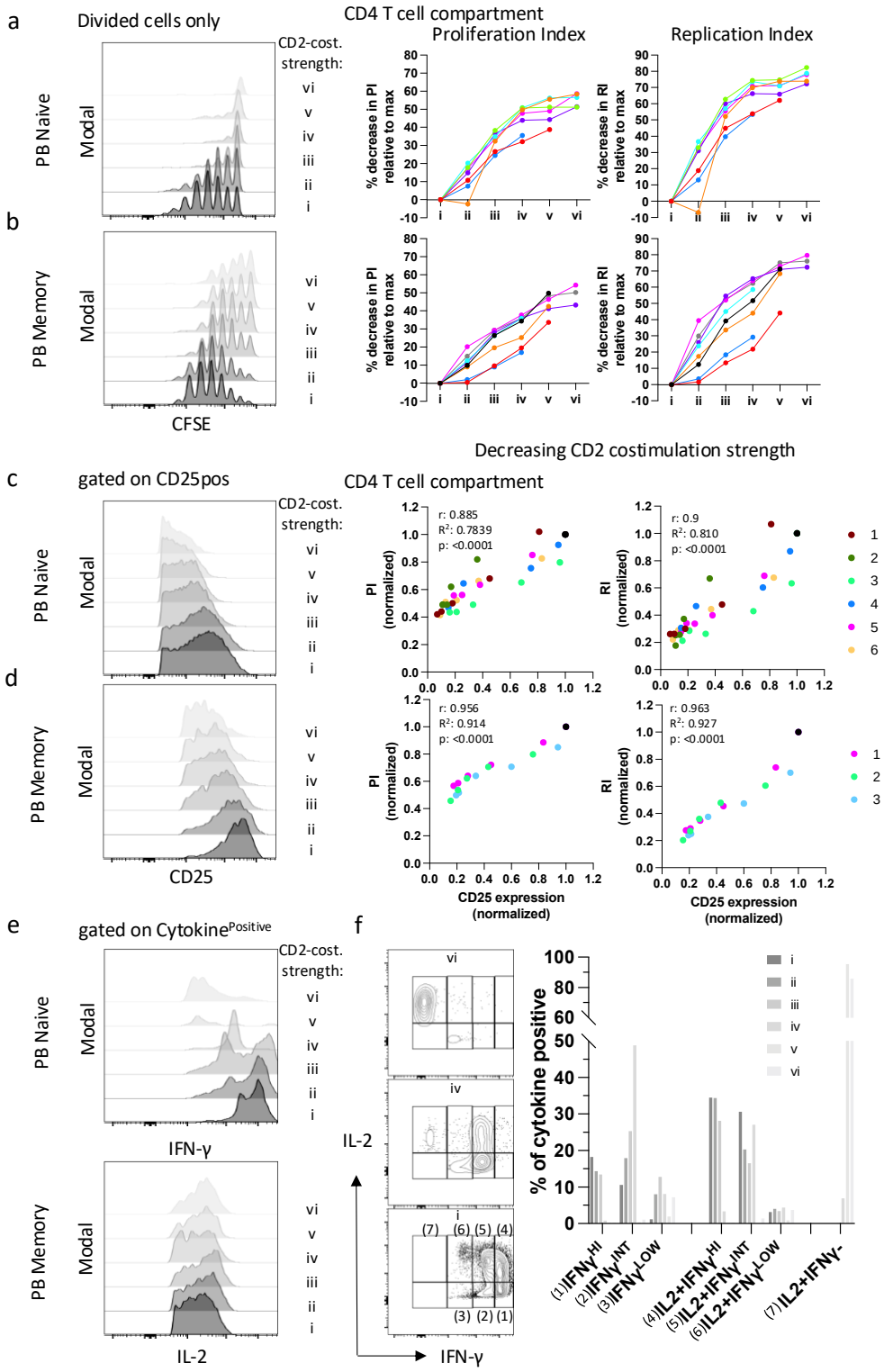

Fig.1. T cell proliferation and IFN-γ production correlate with CD2 costimulation strength. Representative flow cytometry histograms (left) from one healthy volunteer, illustrating cell divisions of PB CFSE-labelled naïve **(a)** and memory **(b)** CD4+ T cells, gated on divided cells and corresponding plots (right) of the percentage decrease in proliferation index and replication index at titrated levels of CD2 costimulation strength (i-vi), 5-days post *in-vitro* activation from 7 donors (each a different colour). From experiments as in (a), representative histograms (left) of CD25 expression in naïve **(c)** and memory **(d)** CD4+ T cells 2 days post *in-vitro* activation, and corresponding plots showing CD25 expression against PI or RI expression for 8 and 3 donors, respectively (all parameters normalized to value in highest CD2 costimulation strength condition (i) to allow pooling of all healthy donors samples in one plot). **(e)** Histograms of intracellular levels of IFN-γ (top) and IL-2 (bottom) expression of naïve CD4+ T cells differentiated to Th1 cells *in-vitro,* 7 days post-activation and **(f)** Quantification of percentages of 7 populations of cytokine producing subsets, as gated in representative IL-2 vs IFN-γ dot plots, in the presence of titrated levels of CD2 costimulation strength (i-vi); a representative donor shown from two independent healthy donor experiments.

Fig 2. A CD2^{low} phenotype exhibited by brain tumour-infiltrating CD8+ and CD4+ T cells.

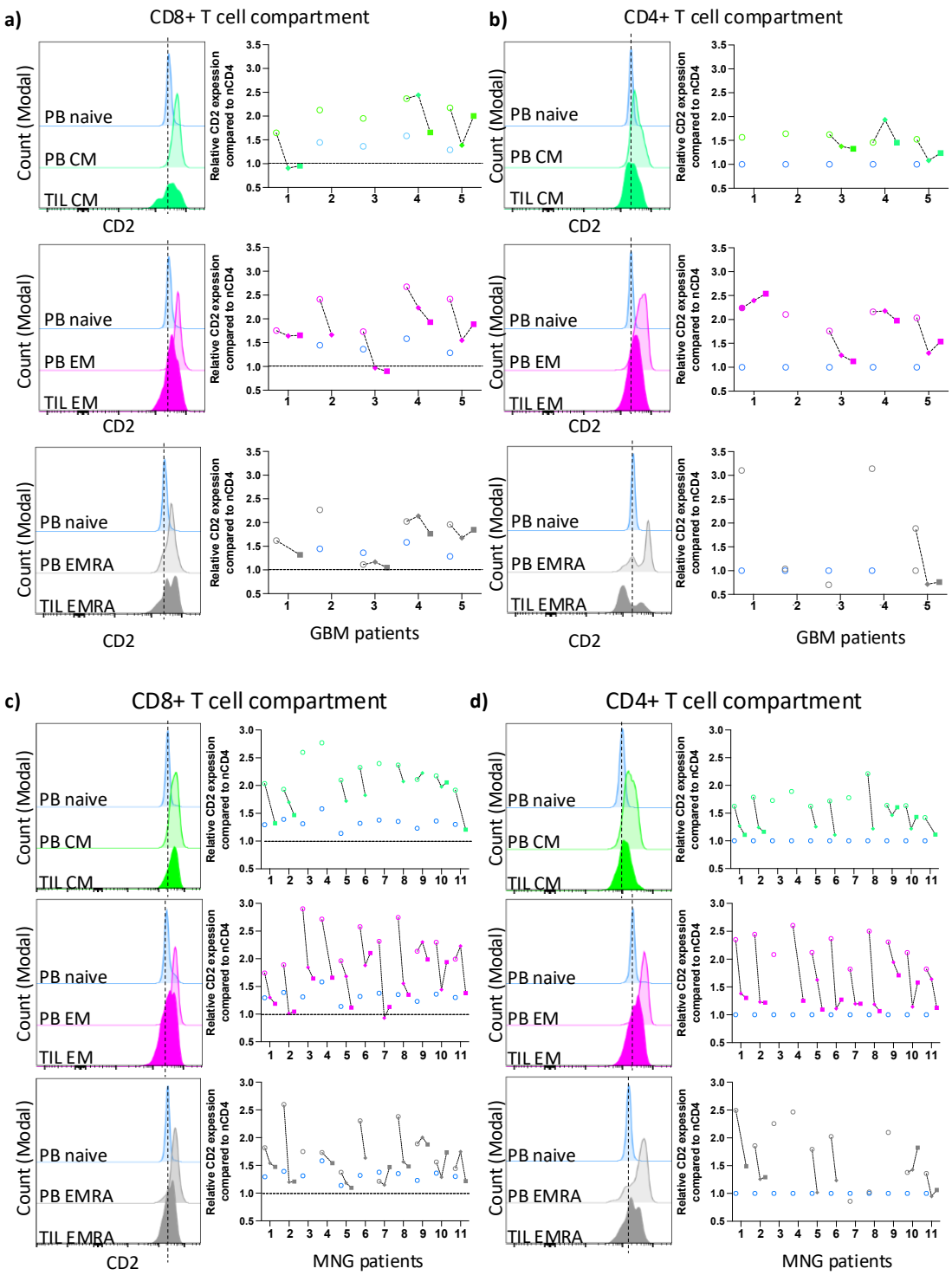

Fig. 2. A CD2^{low} phenotype exhibited by brain tumour infiltrating CD8+ and CD4+ T cells.
(a-b), (left) Representative flow cytometry histogram of CD2 expression in naïve (blue), central memory (CM-green), effector memory (EM-mangenta) and effector-memory re-expressing CD45RA (EMRA-grey) CD8+ and CD4+ T cells, respectively, from peripheral blood (PB-light colour histograms) and tumour (solid colour histograms) from one glioblastoma patient. (**a-b),** (right). Relative CD2 expression in T cell subsets, normalized to CD2 expression in PB naïve CD4+ T cells, per donor per tissue as in (a-b, left) across 5 patients; open-light colour circles represent PB, solid rhombus core side of tumour and solid square peripheral side of tumour. **(c-d)**, Same as in (a-b) but for 11 meningioma patients.

Fig. 3 Genome-scale CRISPR-Cas9 screen identifies positive regulators of CD2.

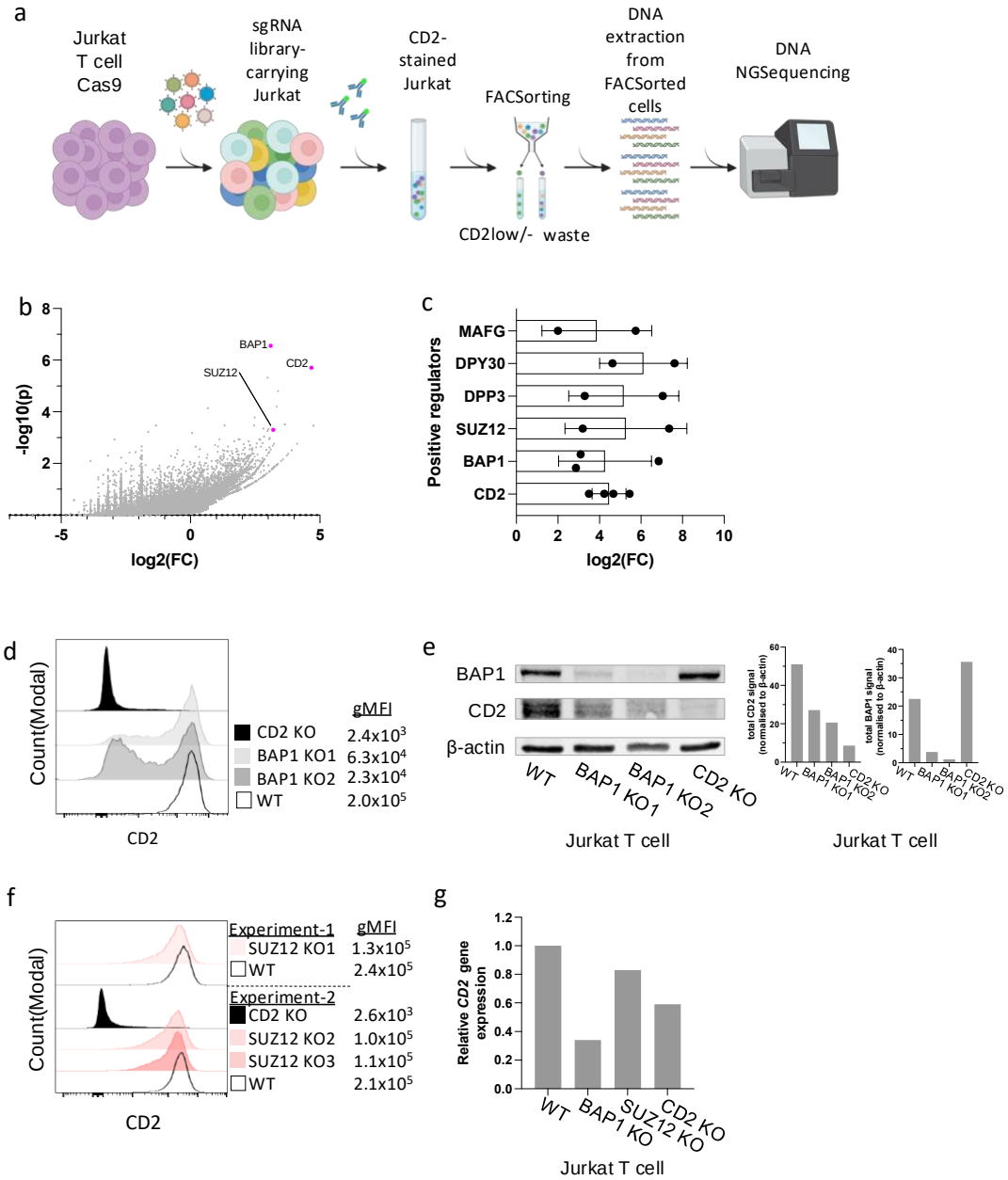

Fig. 3. Genome-scale CRISPR-CAS9 screen identifies positive regulators of CD2.
(a) Diagrams shows the experimental design used for identifying positive regulators of *CD2* using a whole genome-wide CRISPR-CAS9 KO screen in the human Jurkat T cell line. CD2lo expressing cells were FACsorted (step 3) at five different timepoints during the cell library screen culture. **(b)** A representative example plot from one of the timepoints, showing the distribution of target gene enrichment withing the CD2lo population compared to the total unsorted population based on log2 fold change of gene enrichment and p-value for enrichment generated by the use of the MAGeCK algorithm (REF). **(c)** Bar chart showing the log2 fold change enrichment of targeting sgRNAs in CD2lo against unsorted control population, that were reproduced in more than one of the 5 screen timepoints tested; each dot represents a separate timepoint. Data represent mean+/-SD. (**d)** Representative flow cytometry histograms of surface CD2 expression upon two different sgRNA targeting BAP1 for knock out (BAP1 KO1 and KO2) and one sgRNA targeting CD2 (CD2 KO) compared to WT control) and the corresponding geometric mean fluorescence intensity of each total population (gMFI) from two independent experiments. **(e)** Western blot and corresponding bar charts showing the total amount of BAP1 and CD2 protein normalized to beta-actin (b-actin) expression in experiments as in (d). **(f)** Histograms from two independent experiments are presented here, showing the surface CD2 expression upon three different sgRNA targeting SUZ12 for knock out (SUZ1 KO1, KO2 and KO3) compared to a CD2 KO and a WT control with corresponding geometric mean fluorescence intensity of each total population (gMFI). **(g)** Bar chart showing the relative *CD2* mRNA expression upon BAP1, SUZ12 and CD2 KO as in experiments (d-f) compared to WT control as quantified by real-time quantitative PCR.

Fig. 4 CD2 expression is coregulated with expression of markers associated with T cell development, stemness, exhaustion and metabolism

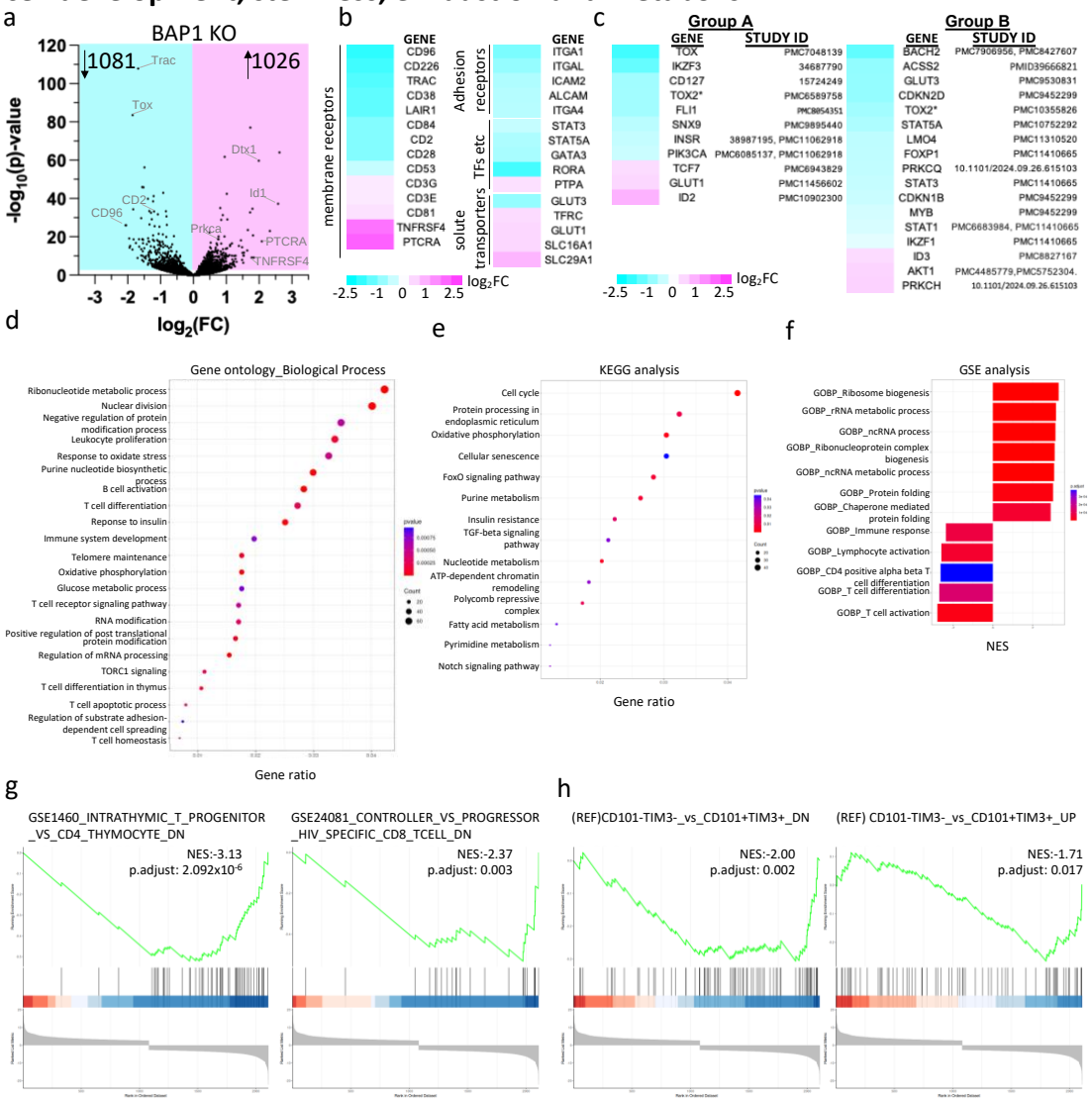

Fig. 4. CD2 expression is coregulated with expression of markers associated with T cell development, stemness, exhaustion and metabolism. (a) Volcano plot showing p value and fold change in expression of genes detected in BAP1 KO Jurkats relative to WT Jurkats. **(b-c)** Heatmap of the log2 fold change (FC) expression of selected differentially expressed genes (DEGs) and their corresponding gene names identified in BAP1 KO Jurkats relative to WT control; these are categorized in T cell surface signaling molecules, adhesion molecules, transcription factors (TF) and solute transporters in (b) and in factors associated with stemness and exhaustion of T cells in (c). **(d-e)** Bubble plots showing a selection of enriched pathways determined by performing gene ontology analysis (biological process pathways) in (d) KEGG pathway analysis in (e) of DEGs in BAP1 KO T cells with a padjust<0.05. The gene count per pathway is represented by the size of the dot and the p value by the colour of the dot. (**f)** Bar chart showing a selection of enriched pathways and the corresponding normalised enrichment score (NES) determined by performing gene set enrichment analysis (GSEA) using the C5 genesets of the Molecular Signatures Database (MSigDB) and the same DEGs as in (d-e). **(g)** A selection of enriched gene signatures in BAP1 KO identified upon GSEA using the C7 immunologica signature gene sets in MSigDB. **(h)** GSEA in BAP1 KO T cells for a progenitor exhausted T cell gene signature generated from [8]

Fig 5. BAP1 has dose-dependent effect on costimulatory receptor expression and stemness-exhaustion transcription factors.

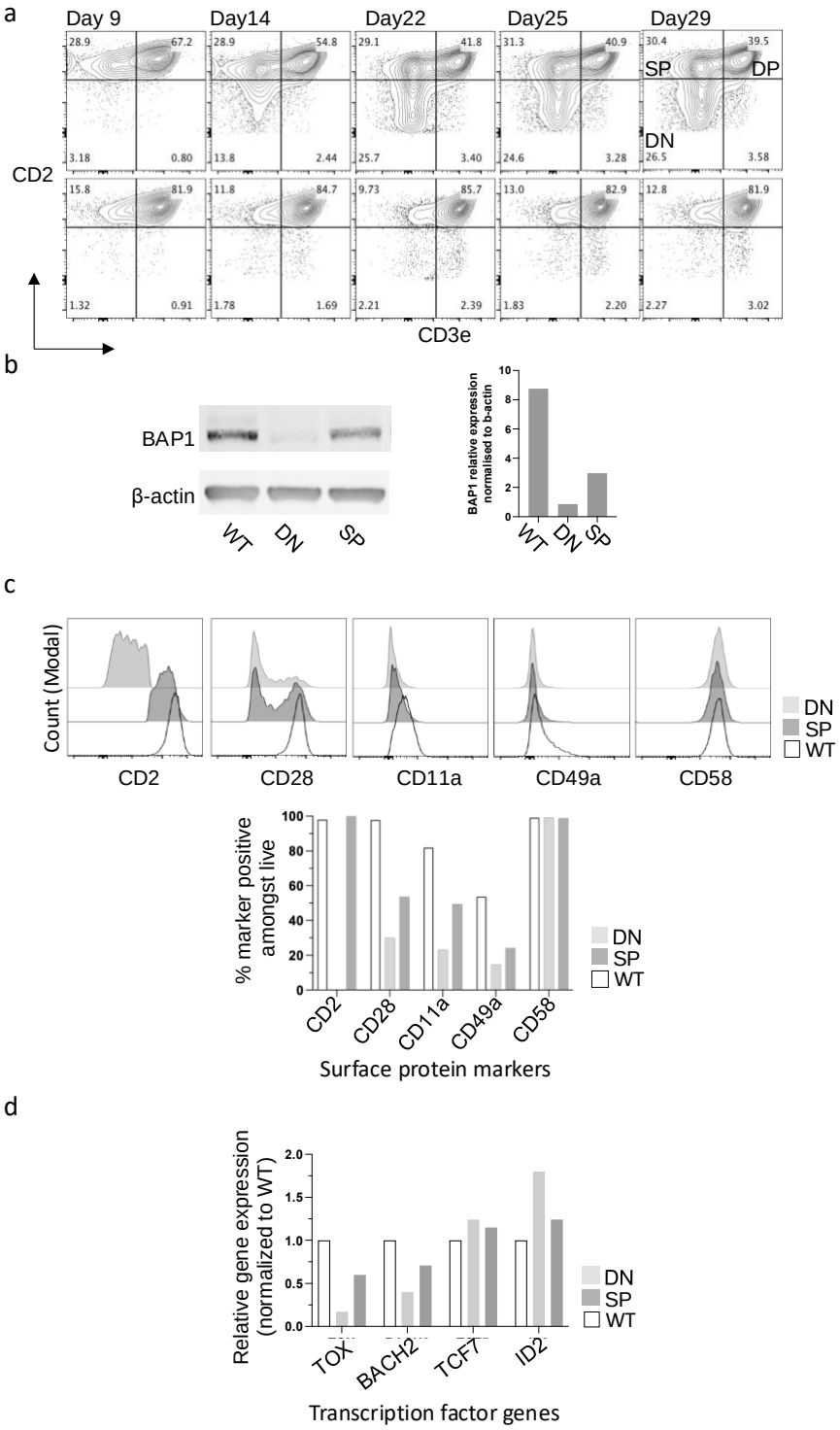

Fig.5. BAP1 has dose-dependent effect on costimulatory receptor expression and stemness-exhaustion transcription factors. (a) Flow cytometry contour plots showing CD2-CD3e expression profile during sgRNA BAP1 KO2 in Jurkat T cells at different timepoints of the culture and the gating to define different populations, double positive, DP: CD3+CD2+, single positive, SP: CD3-CD2+/high, double negative DN: CD3-CD2-/low. (**b)** Western blot and corresponding bar charts showing the total amount of BAP1protein normalized to beta-actin (b-actin) expression in experiments as in (a) at endpoint when culture showed no further deviation in ratio of DP, SP and DN subsets. **(c)** Flow cytometry histograms (top) of CD2, CD28, CD11a, CD49a, CD58 in DN, SP BAP1KO2 T cell subsets and WT T cells and the corresponding percentage positive T cells for each marker is shown in bar chart (bottom). **(d)** Bar chart showing the relative gene expression for stemness-exhaustion associated transcription factors in WT, single positive (SP) and double negative (DN) Jurkats. A reprentative profiling culture timepoint shown out of three.

Fig. 6. T cell activation reveals differential CD2 and TCR expression in BAP1 KO vs WT T cells but not for CD28 and CD226.

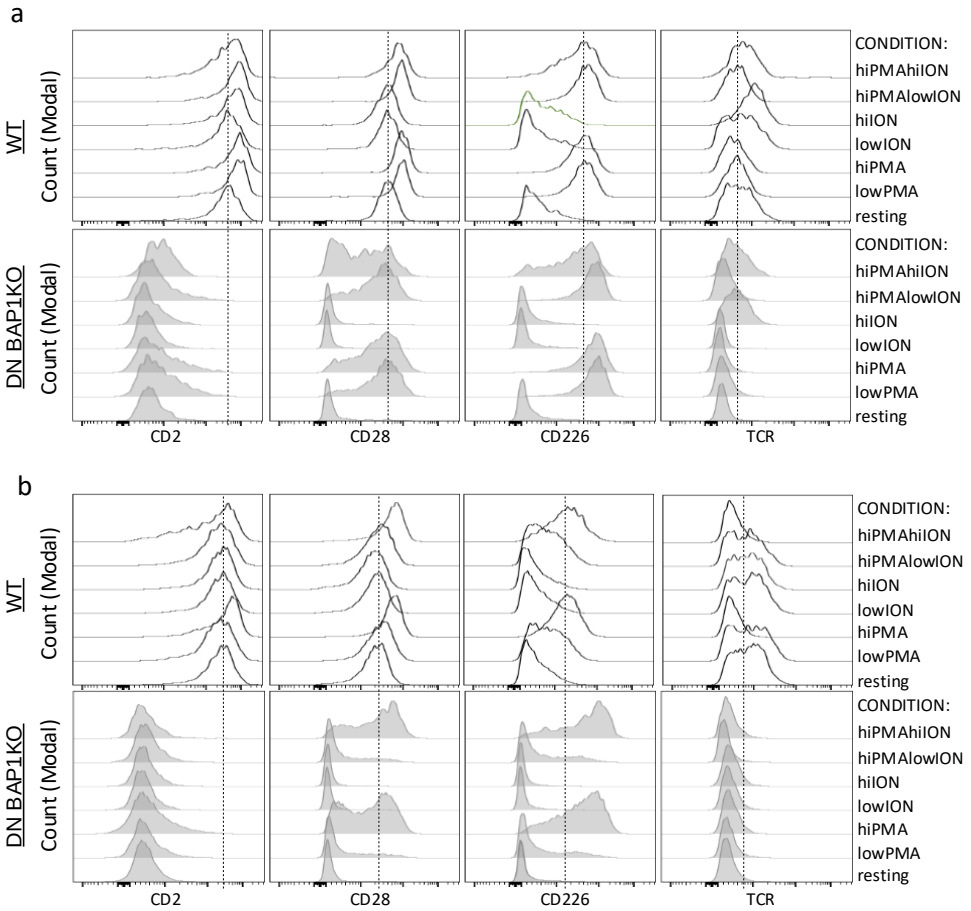

Fig. 6. T cell activation reveals differential CD2 and TCR expression in BAP1 KO vs WT T cells but not for CD28 and CD226. (a) Flow cytometry histograms of CD2, CD28, CD226 and TCR expression in WT and DN BAP1KO T cell in resting conditions and two days post-chemical cell activation by-passing the need to engage the TCR-CD3 complex, with low (0.6µg/ml) and high (20µg/ml) concentrations of phorbol myristate acetate (PMA), with low (0.1µg/ml) and high ((1µg/ml)) concentrations of ionomycin (ION) or a combination of high concentration of PMA with low or high concentration of ION. (**b)** Same as in (a) but 11-12 days post-chemical activation that includes a resting period of cell cultured in no stimulation conditions

Fig. 7 Pharmacological inhibition of histone deacetylases, partially, rescues BAP1 loss-mediated CD2 repression.

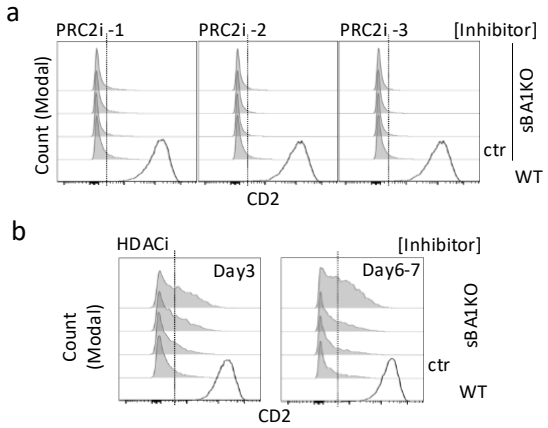

Fig. 7. Pharmacological inhibition of histone deacetylases partially rescues BAP1 loss-mediated CD2 repression. (a) Flow cytometry histograms showing the surface CD2 expression in DN BAP1KO T cells in control condition and upon treatment with three different PRC2 inhibitors in a dose-dependent manner, seven days post-initiation of treatment (PRC2i-1, GSK126, PRC2i-2,A-395, PRC2i-3, Tazemetostat). **(b)** Flow cytometry histograms showing the surface CD2 expression in DN BAP1KO T cells in control condition and upon treatment with HDAC inhibitor, LMK235, in a dose-dependent manner, three and six/seven days post-initiation of treatment; a representative experiment shown from two independent ones.
WT represent CD2 expression in WT T cells in control untreated conditions.